Published in final edited form as:
Biochemistry. 2011 September 20; 50(37): 8018–8027. doi:10.1021/bi201101t.

Crystal Structures of Complexes with Cobalt-Reconstituted Human Arginase I†,,‡

Edward L. D'Antonio and **David W. Christianson***
Roy and Diana Vagelos Laboratories, Department of Chemistry, University of Pennsylvania, Philadelphia, PA 19104-6323

Abstract

The binuclear manganese metalloenzyme human arginase I (HAI) is a potential protein drug for cancer chemotherapy, in that it is capable of depleting extracellular L-Arg levels in the microenvironment of tumor cells that require this nutrient to thrive. Substitution of the native Mn^{2+}_2 cluster with a Co^{2+}_2 cluster in the active site yields an enzyme with enhanced catalytic activity at physiological pH (~7.4) that could serve as an improved protein drug for L-Arg depletion therapy. A different catalytic mechanism is proposed for Co^{2+}_2-HAI compared with that of Mn^{2+}_2-HAI, including an unusual Nε---Co^{2+} coordination mode, to rationalize the lower K_M value of L-Arg and the lower K_i value of L-Orn. However, we now report that no unusual metal coordination modes are observed in the cobalt-reconstituted enzyme: the X-ray crystal structures of unliganded Co^{2+}_2-HAI determined at 2.10 Å resolution (pH 7.0) and 1.97 Å resolution (pH 8.5), as well as the structures of Co^{2+}_2-HAI complexed with the reactive substrate analogue 2(*S*)-amino-6-boronohexanoic acid (ABH, pH 7.0) and the catalytic product L-Orn (pH 7.0) determined at 1.85 Å resolution and 1.50 Å resolution, respectively, are essentially identical to the corresponding structures of Mn^{2+}_2-HAI. Therefore, in the absence of significant structural differences between Co^{2+}_2-HAI and Mn^{2+}_2-HAI, we suggest that a higher concentration of metal-bridging hydroxide ion at physiological pH for Co^{2+}_2-HAI – a consequence of the lower pK_a of a Co^{2+}-bound water molecule compared with a Mn^{2+}-bound water molecule – strengthens electrostatic interactions with cationic amino acids and accounts for enhanced affinity as reflected in the lower K_M value of L-Arg and the lower K_i value of L-Orn.

Arginase is a binuclear manganese metalloenzyme that catalyzes the hydrolysis of L-arginine (L-Arg)[1] to form L-ornithine (L-Orn) and urea (1-5). This metalloenzyme is becoming increasingly prominent in the exploration and development of new approaches to cancer chemotherapy. For example, arginase activity is upregulated in certain human colon cancer and breast cancer cell lines, resulting in decreased L-Arg levels and increased L-Orn levels; since L-Orn is a biosynthetic precursor of polyamines that facilitate tumor cell growth and proliferation, arginase inhibition decreases L-Orn levels and disrupts the L-Orn supply for polyamine biosynthesis, thereby inhibiting cell proliferation (6-9). Conversely, some cancer cells are auxotrophic for L-Arg and depend on extracellular L-Arg to thrive; such cancer cells can be targeted with L-Arg depletion therapy (10, 11). For example, hepatocellular carcinoma cells (12) and prostate carcinoma cells (10, 13) require extracellular L-Arg to

†This work was supported by National Institutes of Health grant GM49758

‡The atomic coordinates and structure factors of metal-free human arginase I, Co^{2+}_2-human arginase I at pH 7.0 and pH 8.5, and Co^{2+}_2-human arginase I complexed with 2(*S*)-amino-6-boronohexanoic acid and L-ornithine have been deposited in the Protein Data Bank (www.rcsb.org) with accession codes 3TF3, 3TH7, 3THE, 3THH, and 3THJ, respectively.

*To whom correspondence should be addressed. D.W.C.: tel, (215) 898-5714; fax, (215) 573-2201; chris@sas.upenn.edu. .

[1]Abbreviations: Mn^{2+}_2-HAI, native human arginase I; Co^{2+}_2-HAI, cobalt-reconstituted human arginase I; L-Arg, L-arginine; L-Orn, L-ornithine; ABH, 2(*S*)-amino-6-boronohexanoic acid; HEPES, *N*-(2-hydroxyethyl)piperazine-*N*'-(2-ethanesulfonic acid).

thrive, in the absence of which they undergo apoptosis (14). Accordingly, arginase is a potential protein drug for cancer chemotherapy insofar that it can efficiently deplete extracellular L-Arg levels in the tumor microenvironment. To this end, the substitution of the native Mn^{2+}_2 cluster with a Co^{2+}_2 cluster in the active site of human arginase I (HAI) yields an enzyme with enhanced catalytic activity at physiological pH (~7.4) that can potentially serve as an even more effective agent for L-Arg depletion therapy (14).

The catalytic mechanism of Mn^{2+}_2-HAI is believed to be initiated by the nucleophilic attack of a metal-bridging hydroxide ion at the guanidinium carbon of L-Arg to form a neutral tetrahedral intermediate, which subsequently collapses to form products L-Orn and urea (Figure 1a) (5, 15, 16). A key feature of this mechanistic proposal is a non-metal binding site for the guanidinium group of L-Arg in the precatalytic enzyme-substrate complex. This hypothesis is consistent with structure-activity relationships established for rat arginase I mutants in which the metal binding sites are perturbed by substitution of the metal ligands (17). These mutants exhibit nearly invariant K_M values regardless of whether Mn^{2+}_A or Mn^{2+}_B binding is perturbed; a more significant effect on K_M would be expected if an inner-sphere substrate-metal coordination interaction occurred in the precatalytic enzyme-substrate complex. This hypothesis is also consistent with the X-ray crystal structures of HAI as well as rat arginase I complexed with boronic acid substrate analogue inhibitors (16, 18). Specifically, the trigonal planar boronic acid moieties of substrate analogues 2(*S*)-amino-6-boronohexanoic acid (ABH) (19) and *S*-(2-boronoethyl)-L-cysteine (20) undergo nucleophilic attack to form negatively charged tetrahedral boronate anions. Each tetrahedral boronate anion coordinates to the Mn^{2+}_2 cluster in the HAI active site in much the same manner expected for the tetrahedral intermediate in catalysis (Figure 1b); a similar binding mode is also observed for 2(*S*)-amino-7-oxoheptanoic acid, an aldehyde amino acid analogue of L-Arg, which binds as the tetrahedral gem-diol (Figure 1c) (21). The geometry required for the binding of such boronic acid or aldehyde hydrates as analogues of the tetrahedral intermediate is not readily compatible with a substrate-metal coordination interaction in the precatalytic enzyme-substrate complex. However, coordination of the Nη2 atom of L-Arg to Mn^{2+}_A can occur during nucleophilic attack: formation of the C–O bond breaks the "Y"-shaped guanidinium π system and localizes a lone electron pair on the Nη2 atom, which can then coordinate to Mn^{2+}_A (Figure 1a) (5).

Curiously, Co^{2+}_2-HAI is proposed to catalyze L-Arg hydrolysis through a significantly different mechanism than Mn^{2+}_2-HAI (14). Specifically, the Nε atom of L-Arg is proposed to coordinate directly to an unspecified Co^{2+} ion in the precatalytic enzyme-substrate complex, after which the Co^{2+}-bound guanidinium group undergoes nucleophilic attack by a hydroxide ion bound to the adjacent Co^{2+} ion to form the tetrahedral intermediate; this intermediate is stabilized by coordination of the Nε and Oη atoms to the Co^{2+} ions and ultimately collapses to yield L-Orn and urea (Figure 1d). This proposal emanates from two observations. First, the K_M of L-Arg at pH 8.5 with Co^{2+}_2-HAI is 11-fold lower than that measured with Mn^{2+}_2-HAI, which implicates the Co^{2+}_2 cluster in a stronger substrate binding interaction. Second, the inhibition constant (K_i) of L-Orn is 26-fold lower than that of L-leucine against Co^{2+}_2-HAI at pH 8.5, whereas the corresponding K_i values are relatively unchanged against Mn^{2+}_2-HAI at pH 8.5. These data are interpreted to suggest that the side chain Nε atom of L-Orn coordinates directly to a Co^{2+} ion (14).

To better understand structure-mechanism relationships in the cobalt-reconstituted enzyme, we now report the X-ray crystal structures of Co^{2+}_2-HAI and its complexes with a boronic acid substrate analogue as well as the catalytic product. Specifically, we describe the structures of metal-free HAI at 1.64 Å resolution, unliganded Co^{2+}_2-HAI at pH 7.0 (2.10 Å resolution) and pH 8.5 (1.97 Å resolution), Co^{2+}_2-HAI complexed with ABH at 1.85 Å resolution, and Co^{2+}_2-HAI complexed with L-Orn at 1.50 Å resolution. These structures

show that Co^{2+} substitution does not trigger any significant structural changes in the active site of HAI. Moreover, these structures do not provide any evidence for different enzyme-substrate, enzyme-intermediate, and enzyme-product binding modes compared with corresponding structures of $Mn^{2+}{}_2$-HAI.

Experimental Procedures

Preparation of Crystalline $Co^{2+}{}_2$-HAI and Complexes

Recombinant HAI was expressed in *Escherichia coli* and purified as described (16), and crystallized in the unliganded state according to published procedures (22). Metal-free HAI crystals were prepared by soaking $Mn^{2+}{}_2$-HAI crystals for 7 days in 15 mM EDTA, 15 mM dipicolinic acid, 100 mM HEPES (pH 7.0), 30% (v/v) Jeffamine ED-2001. Essentially complete metal removal was confirmed by X-ray crystal structure determination, which revealed the absence of both metal ions in the active site. Crystals of metal-free HAI were reconstituted with Co^{2+} at pH 7.0 by soaking in a buffer solution containing 20 mM $CoCl_2$, 100 mM HEPES (pH 7.0), 30% (v/v) Jeffamine ED-2001 for 25 hours. Metal-free HAI crystals were reconstituted with Co^{2+} at pH 8.5 by soaking in 20 mM $CoCl_2$, 100 mM Bicine (pH 8.5), 32% (v/v) Jeffamine ED-2001 for 21 hours. The $Co^{2+}{}_2$-HAI-ABH complex was prepared by soaking a $Co^{2+}{}_2$-HAI crystal in 20 mM ABH, 5 mM $CoCl_2$, 100 mM HEPES (pH 7.0), 30% (v/v) Jeffamine ED-2001 for 39 hours. The $Co^{2+}{}_2$-HAI-L-Orn complex was prepared by soaking a $Co^{2+}{}_2$-HAI crystal in 20 mM L-Orn, 5 mM $CoCl_2$, 0.1 M HEPES (pH 7.0), 30% (v/v) Jeffamine ED-2001 for 24 hours. All crystals were flash-cooled in liquid nitrogen with their corresponding mother liquor solutions serving as cryoprotectants.

X-ray Crystal Structure Determinations

X-ray diffraction data from single crystals of metal-free HAI, $Co^{2+}{}_2$-HAI, the $Co^{2+}{}_2$-HAI-ABH complex, and the $Co^{2+}{}_2$-HAI-L-Orn complex were collected on beamline X29 (λ = 0.9795 Å) of the National Synchrotron Light Source at Brookhaven National Laboratory (Upton, NY). Diffraction data were indexed, integrated, and scaled using the *HKL-2000* suite (23). These twinned arginase crystals belonged to the apparent space group P3, as reported for the $Mn^{2+}{}_2$-HAI-ABH complex (16), and their unit cell dimensions were very similar (Table 1).

Structures were solved by molecular replacement using the program *Phaser* (24) as implemented in *CCP4* (25), with the chain A structure of the $Mn^{2+}{}_2$-HAI-ABH complex (PDB 2AEB) (16) less inhibitor, Mn^{2+} ions, and solvent atoms used as the search probe for rotation and translation function calculations. Each refinement was performed with *CNS* (version 1.2) (26) and model building was performed with *Coot* (version 0.6.1) (27). Hemihedral twinning operation parameters used in the refinement were -h, -k, and l while the twinning fraction depended on the dataset (Table 1).

Crystallographic refinement of each structure against twinned intensity data was performed as previously described (16). Water molecules were included in the later stages of each refinement. For the $Co^{2+}{}_2$-HAI-ABH and $Co^{2+}{}_2$-HAI-L-Orn complexes, gradient omit maps clearly showed ligands bound to the active site of each monomer in the asymmetric unit, and ligand atoms were added and refined with full occupancy. Thermal B factors for ligands were consistent with the average B factor calculated for the entire protein (Table 1). Disordered segments M1–S5 and P320–K322 at the N- and C-termini, respectively, were excluded from all final models. Ramachandran plots revealed Q65 with a disallowed conformation in certain structures. For $Co^{2+}{}_2$-HAI (pH 7.0), this included monomers A and B; in the $Co^{2+}{}_2$-HAI-ABH and $Co^{2+}{}_2$-HAI-L-Orn complexes, this included only monomer A.

Generally speaking, Q65 was characterized by well-defined electron density in these structures, so its conformation was not ambiguous. Moreover, this residue adopted a similar conformation in Mn^{2+}_2-HAI (PDB 2PHA) (22), so its unfavorable conformation was not likely to be an artifact. Data collection and refinement statistics for all structure determinations are recorded in Table 1.

Results

Metal-free HAI

The structure of metal-free HAI is the first structure of any arginase in which both active site metal ions are absent (Figure 2a). The overall structure is comparable to that of unliganded wild-type HAI (Mn^{2+}_2-HAI, PDB 2PHA (22)) with a root-mean-square (r.m.s.) deviation of 0.24 Å for 313 Cα atoms. Metal binding residues D128, D124, H126, D232, D234 and H101 remain fully ordered despite the loss of Mn^{2+}_A and Mn^{2+}_B; however, H101 and D232 undergo slight conformational changes to form a hydrogen bond upon metal dissociation (Figure 2b). Thus, the metal binding site is nearly pre-formed with optimal geometry for metal binding, i.e., minimal conformational changes are necessary for binding the two metal ions required for catalysis.

Co^{2+}_2-HAI

The overall fold of unliganded Co^{2+}_2-HAI at pH 7.0 and pH 8.5 is essentially identical to that of unliganded Mn^{2+}_2-HAI at pH 7.5 (PDB 2PHA (22)), with an r.m.s. deviation of 0.26 Å for 313 Cα atoms or 0.47 Å for 313 Cα atoms, respectively. Interestingly, no metal-bound solvent molecules are observed at pH 7.0, except for a single solvent molecule bound to the Co^{2+}_A ion of chain A (Figure 3a), which could imply weaker coordination or disorder. However, metal-bound solvent molecules are fully visible in the structure of Co^{2+}_2-HAI determined at pH 8.5 (Figure 3b) and are identical to those observed in the structure of unliganded Mn^{2+}_2-HAI (22) (Figure 3c). Parenthetically, we note that a bicine buffer molecule is observed to bind at the mouth of the Co^{2+}_2-HAI active site at pH 8.5 (data not shown).

Co^{2+}_2-HAI-ABH complex

The structure of the Co^{2+}_2-HAI-ABH complex at pH 7.0 is essentially identical to the structure of the Mn^{2+}_2-HAI-ABH complex (PDB 2AEB) (16) in both the overall fold (r.m.s. deviation = 0.25 Å for 313 Cα atoms) and the intermolecular interactions of ABH in the active site. A simulated annealing omit map is shown in Figure 4a along with a superposition of the Mn^{2+}_2-HAI-ABH complex. The boronic acid side chain of ABH undergoes nucleophilic attack, probably by the metal-bridging hydroxide ion, to yield a tetrahedral boronate anion that coordinates to the Co^{2+}_A and Co^{2+}_B ions. The α-carboxylate of ABH accepts hydrogen bonds from N130, S137, and two water molecules, and the α-amino group donates hydrogen bonds to D183 and two water molecules. Water molecules hydrogen bonded with the α-carboxylate and the α-amino groups also hydrogen bond with active site protein residues as summarized in Figure 4b.

Co^{2+}-HAI-L-Orn complex

The structure of the Co^{2+}_2-HAI-L-Orn complex determined at pH 7.0 has an overall fold similar to that of the Mn^{2+}_2-HAI-L-Orn complex determined at pH 6.5 (28), and the r.m.s. deviation for 314 Cα atoms is 0.17 Å. A simulated annealing omit map is shown in Figure 5. The terminal amino group of L-Orn donates hydrogen bonds to D128, the backbone carbonyl of H141, and two solvent molecules, one of which is the metal-bridging hydroxide ion. The α-amino and α-carboxylate groups of L-Orn make interactions similar to those observed for

ABH in the Co^{2+}_2-HAI-ABH complex (Figure 4) and the Mn^{2+}_2-HAI-ABH complex (16). Parenthetically, we note that in the Co^{2+}_2-HAI-L-Orn complex, an additional L-Orn molecule binds to the surface of monomer A in the asymmetric unit, where the backbone carbonyl groups of T134 and T135 accept hydrogen bonds from the α-amino group and the ε-amino group of L-Orn, respectively (data not shown). This second L-Orn molecule is characterized by weak electron density consistent with reduced occupancy; since Stone and colleagues do not report any nonlinearity in product inhibition (14), L-Orn binding to this second site does not appear to significantly affect catalysis.

Discussion

The first successful preparation of a crystalline metal-free arginase described in this work allows for the substitution of metal ions other than the native Mn^{2+} ions in the active site. Previous studies with rat arginase I show that only one Mn^{2+} ion is readily extracted from the Mn^{2+}_2 cluster (29), so the human enzyme offers a distinct advantage for the preparation of the metal-free apoenzyme. Significantly, Co^{2+}_2-HAI is said to have ideal functional properties for use in the treatment of L-Arg auxotrophic tumors, e.g., as assayed against human melanoma and hepatocellular carcinoma cell lines: a decreased pK_a for metal-bound water, a decreased K_M for substrate L-Arg, and a decreased K_i for product L-Orn (14).

Functional studies of Co^{2+}_2-HAI (14) are interpreted to reflect the proposed mechanism in Figure 1d, which includes the following chemical steps: (1) deprotonation of L-Arg, (2) tautomerization of the neutral guanidinium group and coordination of the Nε atom to a Co^{2+} ion, (3) nucleophilic attack at the guanidinium carbon by a Co^{2+}-bound hydroxide ion, (4) formation of the tetrahedral intermediate in which the Oη and Nε atoms are coordinated to separate Co^{2+} ions, (5) collapse of the tetrahedral intermediate to yield product L-Orn with its Nε atom coordinated to one Co^{2+} ion, and a water molecule that displaces urea to coordinate to the other Co^{2+} ion, and (6) ionization of Co^{2+}-bound water to regenerate the nucleophilic Co^{2+}-bound hydroxide ion.

X-ray crystal structures of Co^{2+}_2-HAI allow us to evaluate certain aspects of this mechanistic proposal. First, it is intriguing to consider the possibility that the Nε atom of L-Arg or L-Orn coordinates to an active site metal ion. While it is unusual to consider the inner-sphere coordination of the guanidinium Nε or Nη atom of L-Arg to a metal ion, such interactions are occasionally observed (30). However, since the Nε atom of L-Orn does not coordinate to metal ions in the active site of Co^{2+}_2-HAI (Figure 5) or Mn^{2+}_2-HAI (28), the observed binding mode is at odds with the Nε---Co^{2+} coordination mode proposed for L-Orn, and by inference the Nε---Co^{2+} coordination mode proposed for L-Arg, in Figure 1d (14). Since L-Orn adopts an identical binding mode in the active sites of Mn^{2+}_2-HAI and Co^{2+}_2-HAI (Figure 6), the lower K_i value of L-Orn for binding to Co^{2+}_2-HAI must therefore arise from an indirect effect of the metal ions, e.g., the hydrogen bond between the L-Orn side chain and the metal-bridging solvent molecule (Figure 5). The concentration of metal-bridging hydroxide ion is greater for Co^{2+}_2 than for Mn^{2+}_2 at physiological pH (14), which in turn would strengthen its hydrogen bond and electrostatic interactions with the positively charged side chain of L-Orn.

The binding of ABH as the tetrahedral boronate anion likely mimics the binding of the tetrahedral intermediate and its flanking transition states in catalysis by Mn^{2+}_2-rat arginase I (18), Mn^{2+}_2-HAI (16), Co^{2+}_2-HAI (this work), and Mn^{2+}_2-arginase from *Plasmodium falciparum* (31). The binding conformation of ABH to these enzymes is essentially identical (as illustrated in Figure 6 for Co^{2+}_2-HAI and Mn^{2+}_2-HAI), such that the amino acid side chain is extended into the active site with all C-C bonds adopting trans or nearly trans conformations. Identical binding modes for ABH to these enzymes suggest identical binding

modes for the corresponding tetrahedral intermediate and its flanking transition states, i.e., identical catalytic mechanisms.

Further analysis of the binding mode of ABH to Co^{2+}_2-HAI suggests that the boronate anion hydroxyl groups O2 and O3 correspond to the two hydroxyl groups of the native boronic acid, whereas boronate anion hydroxyl group O1 corresponds to the metal-bridging hydroxide ion of the native enzyme. This binding mode is most consistent with a mechanism in which the trigonal planar boronic acid moiety of ABH (or the trigonal planar guanidinium group of the substrate) enters the active site of Co^{2+}_2-HAI and subsequently undergoes nucleophilic attack by a metal-bridging hydroxide ion to yield the tetrahedral boronate anion (or tetrahedral intermediate), with a metal-bridging hydroxyl group (i.e., the former metal-bridging hydroxide ion) and the terminal O2 hydroxyl group (or Nη2 amino group) coordinated to Co^{2+}_A (Figure 7a). This mechanistic model is identical to that outlined for Mn^{2+}_2-HAI (5) and derives from that initially proposed by Kanyo and colleagues for Mn^{2+}_2-rat arginase I (15), which satisfies the principle of least nuclear motion (Figure 7b) (32). Alternative mechanistic models, such as that initially proposed for Co^{2+}_2-HAI (14), involve additional chemical or conformational steps that would add seemingly unnecessary nuclear motions to the mechanistic sequence.

The observed binding mode of the tetrahedral boronate anion form of ABH to Co^{2+}_2-HAI is not consistent with the proposed binding mode of the tetrahedral intermediate that involves metal coordination by the Nε atom of L-Arg (Figure 1d) (14). A key structural feature that prevents a closer approach of the Nε atom of L-Arg or L-Orn to the binuclear metal cluster is the extensive array of hydrogen bond interactions that anchor the α-amino and α-carboxylate groups of amino acids bound in the arginase active site (e.g., see the scheme summarizing the binding mode of ABH in Figure 4b). This hydrogen bond array ensures the precise molecular recognition of L-amino acids in the arginase active site. Modification or deletion of these enzyme-substrate hydrogen bonds significantly compromises catalysis, either by mutagenesis in the enzyme active site (33) or by modification of substrate structure or stereochemistry (34).

In closing, while the proposed mechanism of Co^{2+}_2-HAI summarized in Figure 1d (14) is inconsistent with the X-ray crystal structures of Co^{2+}_2-HAI reported herein, the fact remains that functional studies clearly indicate a decreased K_M value for substrate L-Arg and a decreased K_i value for product L-Orn (14). If functional differences between Co^{2+}_2-HAI and Mn^{2+}_2-HAI do not arise from structural differences in the binding of substrate, tetrahedral intermediate, and product, from what do they arise? Given that the metal-bridging solvent molecule exhibits a lower pK_a in Co^{2+}_2-HAI, there would be a higher concentration of the negatively charged metal-bridging hydroxide ion at physiological pH in comparison with Mn^{2+}_2-HAI (14). As previously mentioned, this would enhance the hydrogen bond and electrostatic interactions with the positively charged side chain of L-Orn and thereby enhance affinity, which would account for the lower K_i value measured against Co^{2+}_2-HAI. Similarly, we suggest that the lower K_M value measured for L-Arg with Co^{2+}_2-HAI results from an enhanced electrostatic interaction (but not a hydrogen bond interaction) between the positively charged guanidinium side chain of L-Arg and the negatively charged metal-bound hydroxide ion in the precatalytic Michaelis complex. Thus, in the absence of significant structural differences between Mn^{2+}_2-HAI and Co^{2+}_2-HAI complexes, we suggest that a simple electrostatic interaction dependent upon the predominant ionization state of a metal-bound water molecule – not a direct metal coordination interaction – could explain the functional differences between Co^{2+}_2-HAI and Mn^{2+}_2-HAI.

Acknowledgments

We thank the National Synchrotron Light Source at Brookhaven National Laboratory (beamline X29) for access to X-ray crystallographic data collection facilities. Additionally, we thank Drs. Kathryn Cole, Mustafa Köksal, and Patrick Lombardi for helpful discussions.

References

1. Christianson DW, Cox JD. Catalysis by metal-activated hydroxide in zinc and manganese metalloenzymes. Annu. Rev. Biochem. 1999; 68:33–57. [PubMed: 10872443]
2. Ash, DE.; Cox, JD.; Christianson, DW. Arginase: a binuclear manganese metalloenzyme. In: Sigel, A.; Sigel, H., editors. *Manganese and Its Role in Biological Processes*, Vol. 37 of *Metal Ions in Biological Systems*. M. Dekker; New York: 1999. p. 407-428.
3. Morris SM Jr. Regulation of enzymes of the urea cycle and arginine metabolism. Annu. Rev. Nutr. 2002; 22:87–105. [PubMed: 12055339]
4. Ash DE. Structure and function of arginases. J. Nutr. 2004; 134:2760S–2764S. [PubMed: 15465781]
5. Christianson DW. Arginase: structure, mechanism, and physiological role in male and female sexual arousal. Acc. Chem. Res. 2005; 38:191–201. [PubMed: 15766238]
6. Buga GM, Wei LH, Bauer PM, Fukuto JM, Ignarro LJ. N^G-hydroxy-l-arginine and nitric oxide inhibit Caco-2 tumor cell proliferation by distinct mechanisms. Am. J. Physiol. 1998; 275:R1256–R1264. [PubMed: 9756558]
7. Singh R, Pervin S, Karimi A, Cederbaum S, Chaudhuri G. Arginase activity in human breast cancer cell lines: N^{ω}-hydroxy-l-arginine selectivity inhibits cell proliferation and induces apoptosis in MDA-MB-468 cells. Cancer Res. 2000; 60:3305–3312. [PubMed: 10866325]
8. Ochoa AC, Zea AH, Hernandez C, Rodriguez PC. Arginase, prostaglandins, and myeloid-derived suppressor cells in renal cell carcinoma. Clin. Cancer Res. 2007; 13:721s–726s. [PubMed: 17255300]
9. Rodriguez PC, Quiceno DG, Ochoa AC. L-arginine availability regulates T-lymphocyte cell-cycle progression. Blood. 2007; 109:1568–1573. [PubMed: 17023580]
10. Kim RH, Coates JM, Bowles TL, McNerney GP, Sutcliffe J, Jung JU, Gandour-Edwards R, Chuang FYS, Bold RJ, Kung H. Arginine deiminase as a novel therapy for prostate cancer induces autophagy and caspase-independent apoptosis. Cancer Res. 2009; 69:700–708. [PubMed: 19147587]
11. Delage B, Fennell DA, Nicholson L, McNeish I, Lemoine NR, Crook T, Szlosarek PW. Arginine deprivation and argininosuccinate synthetase expression in the treatment of cancer. Int. J. Cancer. 2010; 126:2762–2772. [PubMed: 20104527]
12. Cheng PNM, Leung YC, Lo WH, Tsui SM, Lam KC. Remission of hepatocellular carcinoma with arginine depletion induced by systemic release of endogenous hepatic arginase due to transhepatic arterial embolisation, augmented by high-dose insulin: arginase as a potential drug candidate for hepatocellular carcinoma. Cancer Lett. 2005; 224:67–80. [PubMed: 15911102]
13. Dillon BJ, Prieto VG, Curley SA, Ensor CM, Holtsberg FW, Bomalaski JS, Clark MA. Incidence and distribution of argininosuccinate synthetase deficiency in human cancers: a method for identifying cancers sensitive to arginine deprivation. Cancer. 2004; 100:826–833. [PubMed: 14770441]
14. Stone EM, Glazer ES, Chantranupong L, Cherukuri P, Breece RM, Tierney DL, Curley SA, Iverson BL, Georgiou G. Replacing Mn^{2+} with Co^{2+} in human arginase I enhances cytotoxicity toward l-arginine auxotrophic cancer cell lines. ACS Chem. Biol. 2010; 5:333–342. [PubMed: 20050660]
15. Kanyo ZF, Scolnick LR, Ash DE, Christianson DW. Structure of a unique binuclear manganese cluster in arginase. Nature. 1996; 383:554–557. [PubMed: 8849731]
16. Di Costanzo L, Sabio G, Mora A, Rodriguez PC, Ochoa AC, Centeno F, Christianson DW. Crystal structure of human arginase I at 1.29-Å resolution and exploration of inhibition in the immune response. Proc. Natl. Acad. Sci. U. S. A. 2005; 102:13058–13063. [PubMed: 16141327]

17. Cama E, Emig FA, Ash DE, Christianson DW. Structural and functional importance of first-shell metal ligands in the binuclear manganese cluster of arginase I. Biochemistry. 2003; 42:7748–7758. [PubMed: 12820884]
18. Cox JD, Kim NN, Traish AM, Christianson DW. Arginase-boronic acid complex highlights a physiological role in erectile function. Nat. Struct. Biol. 1999; 6:1043–1047. [PubMed: 10542097]
19. Baggio R, Elbaum D, Kanyo ZF, Carroll PJ, Cavalli RC, Ash DE, Christianson DW. Inhibition of Mn^{2+}_2-arginase by borate leads to the design of a transition state analogue inhibitor, 2(*S*)-amino-6-boronohexanoic acid. J. Am. Chem. Soc. 1997; 119:8107–8108.
20. Kim NN, Cox JD, Baggio RF, Emig FA, Mistry SK, Harper SL, Speicher DW, Morris SM, Ash DE, Traish A, Christianson DW. Probing erectile function: *S*-(2-boronoethyl)-l-cysteine binds to arginase as a transition state analogue and enhances smooth muscle relaxation in human penile corpus cavernosum. Biochemistry. 2001; 40:2678–2688. [PubMed: 11258879]
21. Shin H, Cama E, Christianson DW. Design of amino acid aldehydes as transition-state analogue inhibitors of arginase. J. Am. Chem. Soc. 2004; 126:10278–10284. [PubMed: 15315440]
22. Di Costanzo L, Pique ME, Christianson DW. Crystal structure of human arginase I complexed with thiosemicarbazide reveals an unusual thiocarbonyl μ-sulfide ligand in the binuclear manganese cluster. J. Am. Chem. Soc. 2007; 129:6388–6389. [PubMed: 17469833]
23. Otwinowski Z, Minor W. Processing of X-ray diffraction data collected in oscillation mode. Methods Enzymol. 1997; 276:307–326.
24. McCoy AJ, Grosse-Kunstleve RW, Storoni LC, Read RJ. Likelihood-enhanced fast translation functions. Acta Crystallogr., Sect. D: Biol. Crystallogr. 2005; 61:458–464. [PubMed: 15805601]
25. Collaborative Computational Project, No. 4. The CCP4 suite: programs for protein crystallography. Acta Crystallogr., Sect. D: Biol. Crystallogr. 1994; 50:760–763. [PubMed: 15299374]
26. Brünger AT, Adams PD, Clore GM, Delano WL, Gros P, Grosse-Kunstleve RW, Jiang JS, Kuszewski J, Nilges N, Pannu NS, Read RJ, Rice LM, Simonson T, Warren GL. Crystallography and NMR system (CNS): a new software system for macromolecular structure determination. Acta Crystallogr., Sect. D: Biol. Crystallogr. 1998; 54:905–921. [PubMed: 9757107]
27. Emsley P, Cowtan K. Coot: model-building tools for molecular graphics. Acta Crystallogr., Sect. D: Biol. Crystallogr. 2004; 60:2126–2132. [PubMed: 15572765]
28. Ilies M, Di Costanzo L, Dowling DP, Thorn KJ, Christianson DW. Binding of α,α-disubstituted amino acids to arginase suggests new avenues for inhibitor design. J. Med. Chem. 2011; 54:5432–5443. [PubMed: 21728378]
29. Scolnick LR, Kanyo ZF, Cavalli RC, Ash DE, Christianson DW. Altering the binuclear manganese cluster of arginase diminishes thermostability and catalytic function. Biochemistry. 1997; 36:10558–10565. [PubMed: 9265637]
30. Di Costanzo L, Flores LV, Christianson DW. Stereochemistry of guanidine-metal interactions: implications for l-arginine-metal interactions in protein structure and function. Proteins: Struct., Funct., Bioinf. 2006; 65:637–642.
31. Dowling DP, Ilies M, Olszewski KL, Portugal S, Mota MM, Llinás M, Christianson DW. Crystal structure of arginase from *Plasmodium falciparum* and implications for l-arginine depletion in malarial infection. Biochemistry. 2010; 49:5600–5608. [PubMed: 20527960]
32. Hine J. The principle of least nuclear motion. Adv. Phys. Org. Chem. 1978; 15:1–61.
33. Shishova EY, Di Costanzo L, Emig FA, Ash DE, Christianson DW. Probing the specificity determinants of amino acid recognition by arginase. Biochemistry. 2009; 48:121–131. [PubMed: 19093830]
34. Reczkowski RS, Ash DE. Rat liver arginase: kinetic mechanism, alternate substrates, and inhibitors. Arch. Biochem. Biophys. 1994; 312:31–37. [PubMed: 8031143]
35. Laskowski RA, MacArthur MW, Moss DS, Thornton JM. PROCHECK: a program to check the stereochemical quality of protein structures. J. Appl. Crystallogr. 1993; 26:283–291.
36. Kleywegt, GJ.; Zou, JY.; Kjeldgaard, M.; Jones, TA. Around O, in *International Tables for Crystallography*. Rossmann, MG.; Arnold, E., editors. Kluwer Academic Publishers; Dordrecht (Netherlands): 2001. p. 353-356.p. 366-367.

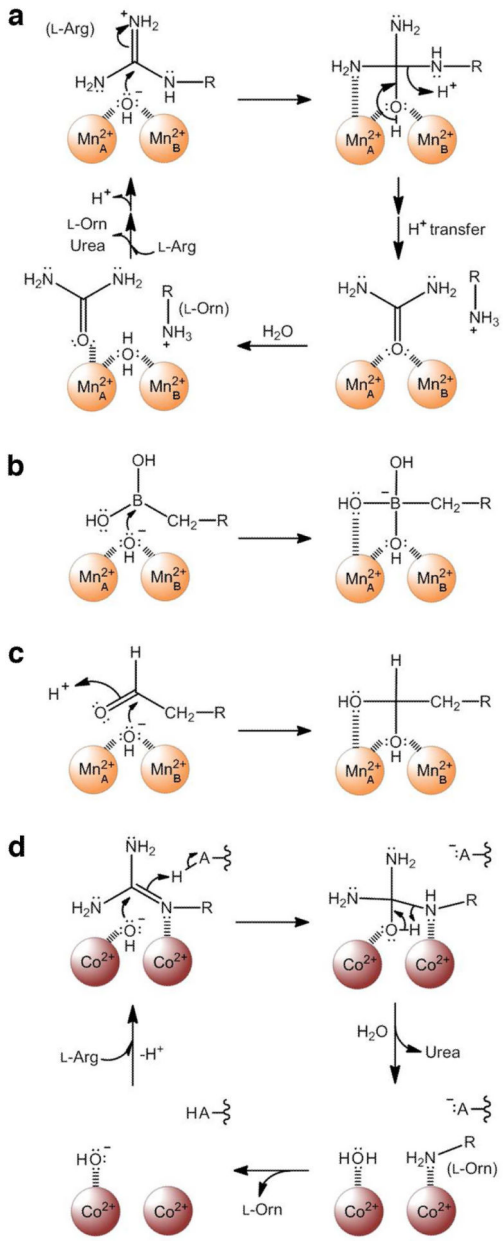

Figure 1.

(a) Proposed mechanism of Mn^{2+}_2-HAI (5). (b) The binding of a boronic acid inhibitor as the tetrahedral boronate anion mimics the tetrahedral intermediate and its flanking transition states in catalysis (16, 18, 20). (c) The binding of an aldehyde inhibitor as the tetrahedral gem-diol mimics the tetrahedral intermediate and its flanking transition states in catalysis (21). (d) Proposed mechanism of Co^{2+}_2-HAI (14).

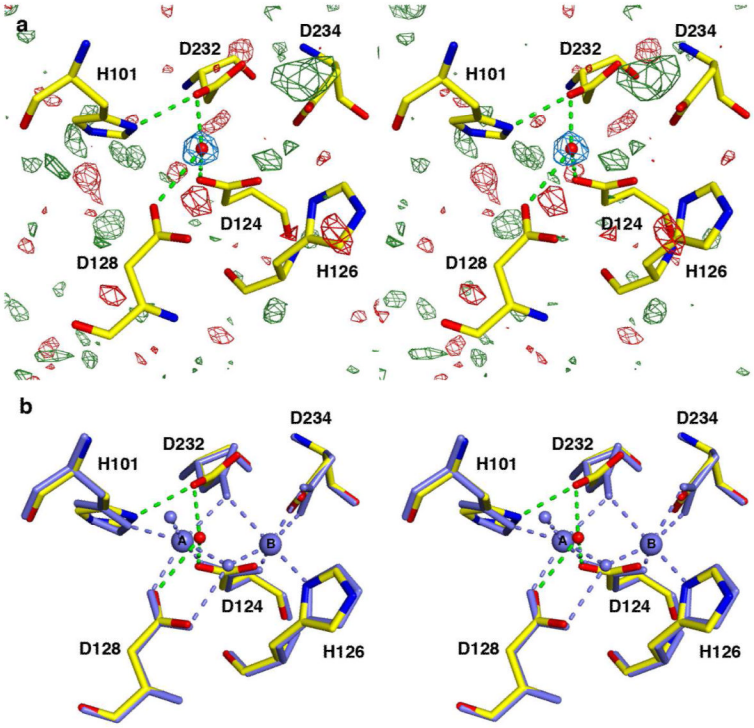

Figure 2.

(a) Final $|F_o|$ - $|F_c|$ map of metal-free HAI contoured at 3.0σ (green) and −3.0σ (red). Only spurious noise peaks are observed, and none correspond to residual metal ions. A water molecule (red sphere), confirmed in a simulated annealing omit map contoured at 3.0σ (blue), is hydrogen bonded (green dashed lines) to D124, D128, and D232. Atoms are color-coded as follows: C = yellow, N = blue, O = red. (b) Superposition of chains A for metal-free HAI (pH 7.0, color-coded as in (a)) and $Mn^{2+}{}_2$-HAI (pH 7.5) (PDB 2PHA, all atoms and interactions colored light blue). Apart from small conformational changes of D232 and H101, protein residues in the apoenzyme are nearly pre-formed for ideal metal coordination interactions.

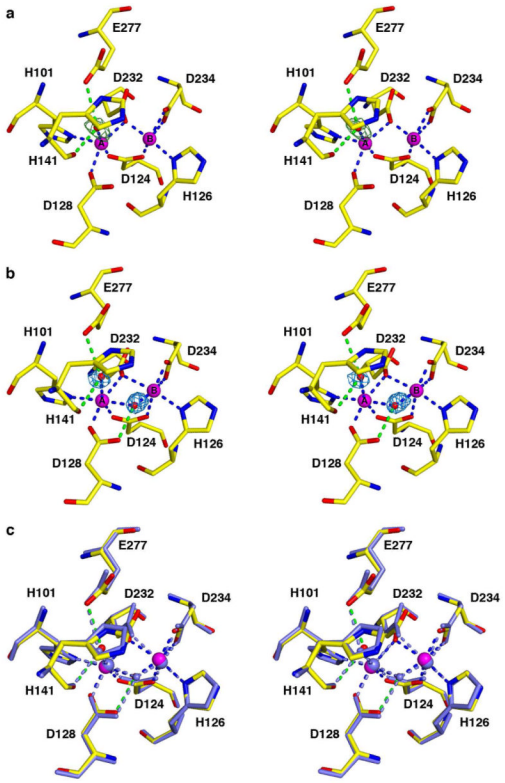

Figure 3.

(a) Simulated annealing omit map (green) of the Co^{2+}_{A}-bound solvent molecule in chain A of Co^{2+}_{2}-HAI at pH 7.0, contoured at 3.5σ. Atoms are color-coded as follows: C = yellow, N = blue, O = red, Co^{2+} = magenta spheres, solvent = red sphere. Metal coordination and hydrogen bond interactions appear as blue and green dashed lines, respectively. (b) Simulated annealing omit map (blue) of the Co^{2+}-bound solvent molecules in Co^{2+}_{2}-HAI at pH 8.5, contoured at 4.2σ. Atoms and intermolecular interactions are color-coded as in (a). (c) Superposition of chains A for Co^{2+}_{2}-HAI (pH 8.5) (color-coded as in (b)) and Mn^{2+}_{2}-HAI (pH 7.5) (PDB 2PHA, all atoms light blue).

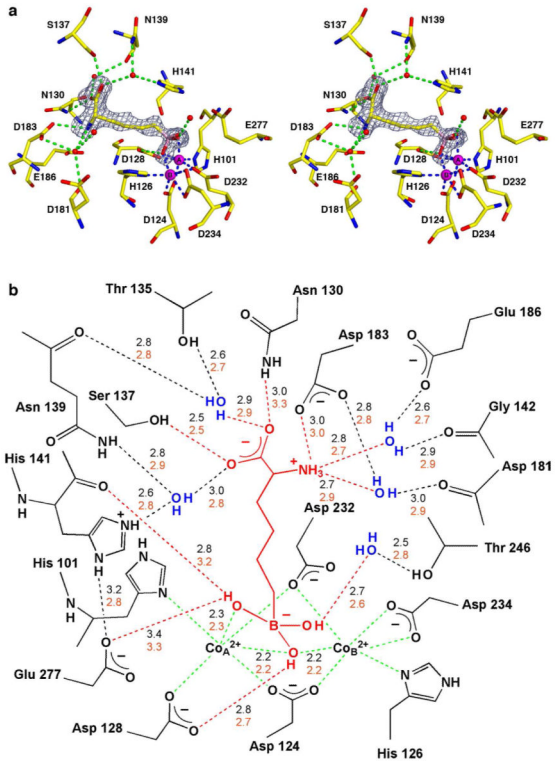

Figure 4.

(a) Simulated annealing omit map (grey) of the inhibitor ABH bound in the active site of Co^{2+}_2-HAI, contoured at 4.0σ. The boronic acid moiety of ABH binds as a tetrahedral boronate anion that mimics the tetrahedral intermediate and its flanking transition states in the reaction catalyzed by Co^{2+}_2-HAI. Atoms are color-coded as follows: C = yellow, N = blue, O = red, B = pink, Co^{2+} = magenta spheres, solvent = red spheres; metal coordination and hydrogen bond interactions are indicated by blue and green dashed lines, respectively. (b) Scheme illustrating average distances (Å) of intermolecular interactions in the Co^{2+}_2-HAI-ABH complex (black numbers) and Mn^{2+}_2-HAI-ABH complex (PDB 2AEB) (orange numbers).

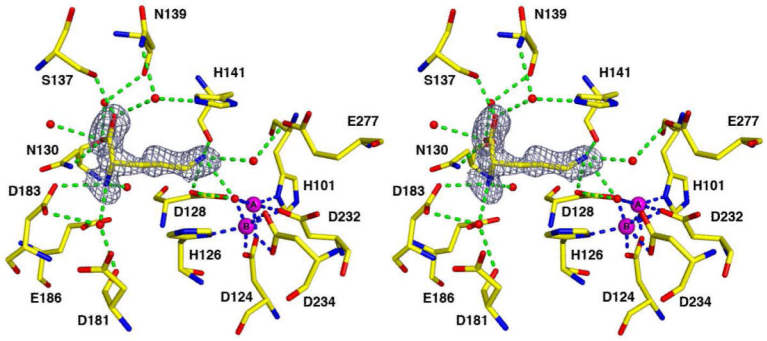

Figure 5.

Simulated annealing omit map (grey) of the catalytic product L-Orn bound in the active site of Co^{2+}_2-HAI at pH 7.0, contoured at 3.0σ. Atoms are color-coded as follows: C = yellow, N = blue, O = red, Co^{2+} = magenta spheres, solvent = red spheres; metal coordination and hydrogen bond interactions are indicated by blue and green dashed lines, respectively.

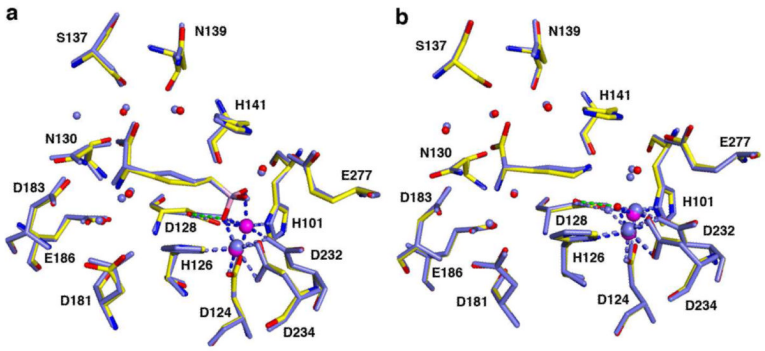

Figure 6.

(a) Superposition of the Co^{2+}_2-HAI-ABH complex (color-coded as in Figure 4a) and the Mn^{2+}_2-HAI-ABH complex at pH 7.5 (PDB 2AEB, all atoms and metal coordination interactions light blue). Apart from a 0.5 Å shift of the side chain Cγ atom of ABH, the structures of these complexes are essentially identical. (b) Superposition of the Co^{2+}_2-HAI-$_L$-Orn complex (color-coded as in Figure 5) and the Mn^{2+}_2-HAI-$_L$-Orn complex (PDB 3GMZ, all atoms and interactions light blue).

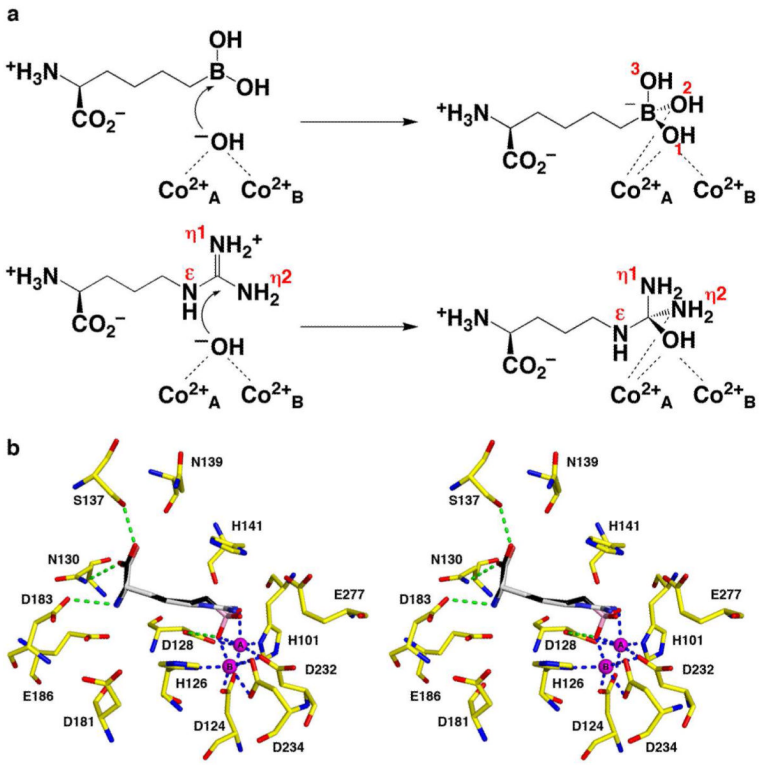

Figure 7.

(a) Attack of the nucleophilic metal-bridging hydroxide ion at the boronic acid moiety of the inhibitor ABH results in the formation of a tetrahedral boronate anion that mimics the formation of the tetrahedral intermediate in catalysis. While this chemistry is illustrated for Co^{2+}_2-HAI, it is identical to that of Mn^{2+}_2-HAI. Selected atoms discussed in the text are indicated with red labels. (b) Model of L-Arg superimposed on the experimentally determined structure of ABH bound in the active site of Co^{2+}_2-HAI, which mimics the binding of the tetrahedral intermediate and its flanking transition states in catalysis. Atoms are color-coded as follows: C = yellow (protein), black (ABH), or grey (L-Arg), N = blue, O = red, Co^{2+} = magenta spheres. Solvent molecules are omitted for clarity; metal coordination and hydrogen bond interactions for ABH are indicated by blue and green dashed lines, respectively. The side chain Nη1 and Nη2 atoms of L-Arg correspond to the boronate O3 and O2 atoms (atom labels are shown in (a)). Nucleophilic attack of a metal-bridging hydroxide ion (which would correspond to the position of the boronate O1 atom) at the planar guanidinium group of L-Arg satisfies the principle of least nuclear motion, and simply requires the pyramidalization of the guanidinium carbon (or the boron atom of the boronic acid) as it transitions from sp^2 to sp^3 hybridization. This conclusion is valid for both Co^{2+}_2-HAI and Mn^{2+}_2-HAI.

Table 1

Data collection and refinement statistics

		Co^{2+}_2-HAI			
	metal-free HAI	**pH 7.0**	**pH 8.5**	**Co^{2+}_2-HAI-ABH**	**Co^{2+}_2-HAI-L-Orn**
Data collection					
resolution limits (Å)	50.0 - 1.64	50.0 - 2.10	50.0 - 1.97	50.0 - 1.85	50.0 - 1.50
total/unique reflections measured	837181/78451	174332/37395	179056/40321	247148/53857	558194/102235
unit cell dimensions					
a, b, c (Å)	90.86, 90.86, 69.88	90.41, 90.41, 69.74	87.42, 87.42, 67.25	90.43, 90.43, 69.43	90.49, 90.49, 69.69
α, β, γ (deg)	90, 90, 120	90, 90, 120	90, 90, 120	90, 90, 120	90, 90, 120
R_{merge} [a,b]	0.080 (0.430)	0.126 (0.417)	0.097 (0.608)	0.078 (0.586)	0.109 (0.550)
$I/\sigma(I)$ [a]	35.18 (5.46)	12.25 (4.18)	14.98 (2.20)	19.55 (2.32)	14.63 (2.89)
completeness (%) [a]	99.3 (95.4)	100 (100)	98.9 (96.3)	99.3 (98.4)	99.9 (100)
Refinement					
reflections used in refinement/test set	70907/6432	34308/1833	36032/1913	46410/5045	94996/4852
twinning fraction	0.50	0.45	0.30	0.50	0.45
R_{twinc} [c]	0.155	0.147	0.144	0.195	0.148
$R_{twin/free}$ [c]	0.197	0.209	0.193	0.239	0.178
solvent molecules [d]	207	127	223	233	277
ligand molecules [d]	0	0	2	2	3
Co^{2+} ions [d]	0	4	4	4	4
Root mean square deviations [e]					
bonds (Å)	0.008	0.008	0.007	0.007	0.007
angles (deg)	1.5	1.5	1.5	1.5	1.6
Average B-factors (Å²) [f]					
main chain	24	24	24	27	20

		Co^{2+}_2-HAI			
	metal-free HAI	**pH 7.0**	**pH 8.5**	**Co^{2+}_2-HAI-ABH**	**Co^{2+}_2-HAI-L-Orn**
side chain	26	25	26	28	21
solvent	26	24	28	28	23
ligand	--	--	36	22	23
Co^{2+} ions	--	20	25	20	15
Ramachandran plot (%) [e]					
allowed	89.2	85.7	88.4	86.9	90.4
additionally allowed	10.2	13.9	11.2	12.7	9.2
generously allowed	0.6	0.0	0.4	0.2	0.2
disallowed	0.0	0.4	0.0	0.2	0.2
PDB accession code	3TF3	3TH7	3THE	3THH	3THJ

[a] Values in parenthesis are for the highest resolution shell.

[b] $R_{merge} = \Sigma |I - \langle I \rangle| / \Sigma I$, where I is the observed intensity and $\langle I \rangle$ is the average intensity calculated from replicate data.

[c] $R_{twin} = \Sigma |[|F_{calc/A}|^2 + |F_{calc/B}|^2]^{1/2} - |F_{obs}|| / \Sigma |F_{obs}|$ for reflections contained in the working set. $|F_{obs}|$ is the observed structure factor amplitude, and $|F_{calc/A}|$ and $|F_{calc/B}|$ are the structure factor amplitudes calculated for twin domains A and B, respectively. R_{twin} underestimates the residual error in the model over the two twin-related reflections by a factor of approximately 0.7. The same expression describes $R_{twin/free}$, calculated for test set reflections excluded from refinement.

[d] Per asymmetric unit cell

[e] Calculated using *PROCHECK* (35)

[f] Calculated using *MOLEMAN* (36)